



OPEN

LTP of inhibition at PV interneuron output synapses requires developmental BMP signaling

Evan Vickers^{1,3}, Denys Osypenko¹, Christopher Clark^{1,4}, Zeynep Okur², Peter Scheiffele² & Ralf Schneggenburger¹✉

Parvalbumin (PV)-expressing interneurons (PV-INs) mediate well-timed inhibition of cortical principal neurons, and plasticity of these interneurons is involved in map remodeling of primary sensory cortices during critical periods of development. To assess whether bone morphogenetic protein (BMP) signaling contributes to the developmental acquisition of the synapse- and plasticity properties of PV-INs, we investigated conditional/conventional double KO mice of BMP-receptor 1a (BMPR1a; targeted to PV-INs) and 1b (BMPR1a/1b (c)DKO mice). We report that spike-timing dependent LTP at the synapse between PV-INs and principal neurons of layer 4 in the auditory cortex was absent, concomitant with a decreased paired-pulse ratio (PPR). On the other hand, baseline synaptic transmission at this connection, and action potential (AP) firing rates of PV-INs were unchanged. To explore possible gene expression targets of BMP signaling, we measured the mRNA levels of the BDNF receptor TrkB and of P/Q-type Ca²⁺ channel α -subunits, but did not detect expression changes of the corresponding genes in PV-INs of BMPR1a/1b (c)DKO mice. Our study suggests that BMP-signaling in PV-INs during and shortly after the critical period is necessary for the expression of LTP at PV-IN output synapses, involving gene expression programs that need to be addressed in future work.

The neocortex of mammals contains specific classes of excitatory and inhibitory neurons^{1–4}. Amongst the inhibitory interneurons, PV-INs can sustain high - frequency AP firing, and show fast membrane potential signaling and temporal precision at their input - and output synapses⁵. PV-INs form output synapses largely on soma-near compartments of principal neurons⁶, and the resulting GABA release causes well-timed inhibition of cortical principal neurons^{7,8}. Furthermore, the output synapses of PV-INs can undergo long-term potentiation^{9–11} as well as long-term depression (LTD; ref. ¹¹). Plasticity of inhibition, in part provided by PV-INs, has been related to critical period plasticity in the visual^{9,12,13}, somatosensory¹⁴ and auditory cortex¹¹. It is likely that the physiological properties of PV-INs are gradually acquired during postnatal development¹⁵, driven by specific gene expression changes¹⁶. Nevertheless, little is known about the molecular mechanisms which determine the developmental acquisition of the physiological properties of PV-INs, including their fast firing properties, synaptic connectivity, and the plasticity at their output synapses.

Here, we investigate a possible role of BMP-receptor signaling for the development of these functional properties of PV-INs. BMPs are members of the TGF-beta superfamily of growth factors, with widespread roles for the embryonic development and patterning of various mammalian tissues^{17–19}, including the nervous system^{20,21}. In the mammalian CNS, BMP-receptors (BMPRs) and their ligands are expressed up to early adulthood^{22–24}, suggesting that BMP signaling fulfills further roles in later brain development. Indeed, a role for BMP signaling in the elimination of excitatory synapses^{25,26} and in the development of mono-innervation at a large excitatory connection in the auditory brainstem, has been reported^{27,28}. Earlier genetic studies showed that BMP signaling drives the growth of motor nerve terminals at the *Drosophila* neuromuscular junction^{29–31}. Together, these studies suggest a role for BMP signaling in guiding the establishment of specific synaptic connectivity at excitatory connections in the mammalian brain and in the periphery.

Evidence for a role of BMP signaling in the development of inhibitory interneurons is also emerging. A previous study showed that BMP-signaling in the OLIG lineage of neuronal/oligodendrocyte precursors determines

¹Laboratory of Synaptic Mechanisms, Brain Mind Institute, School of Life Science, École Polytechnique Fédérale de Lausanne (EPFL), 1015, Lausanne, Switzerland. ²Biozentrum, University of Basel, 4056, Basel, Switzerland. ³Present address: Institute of Neuroscience, University of Oregon, Eugene, OR, 97403, USA. ⁴Present address: Institute for Regenerative Medicine, University of Zürich, 8952, Schlieren, Switzerland. ✉e-mail: ralf.schneggenburger@epfl.ch

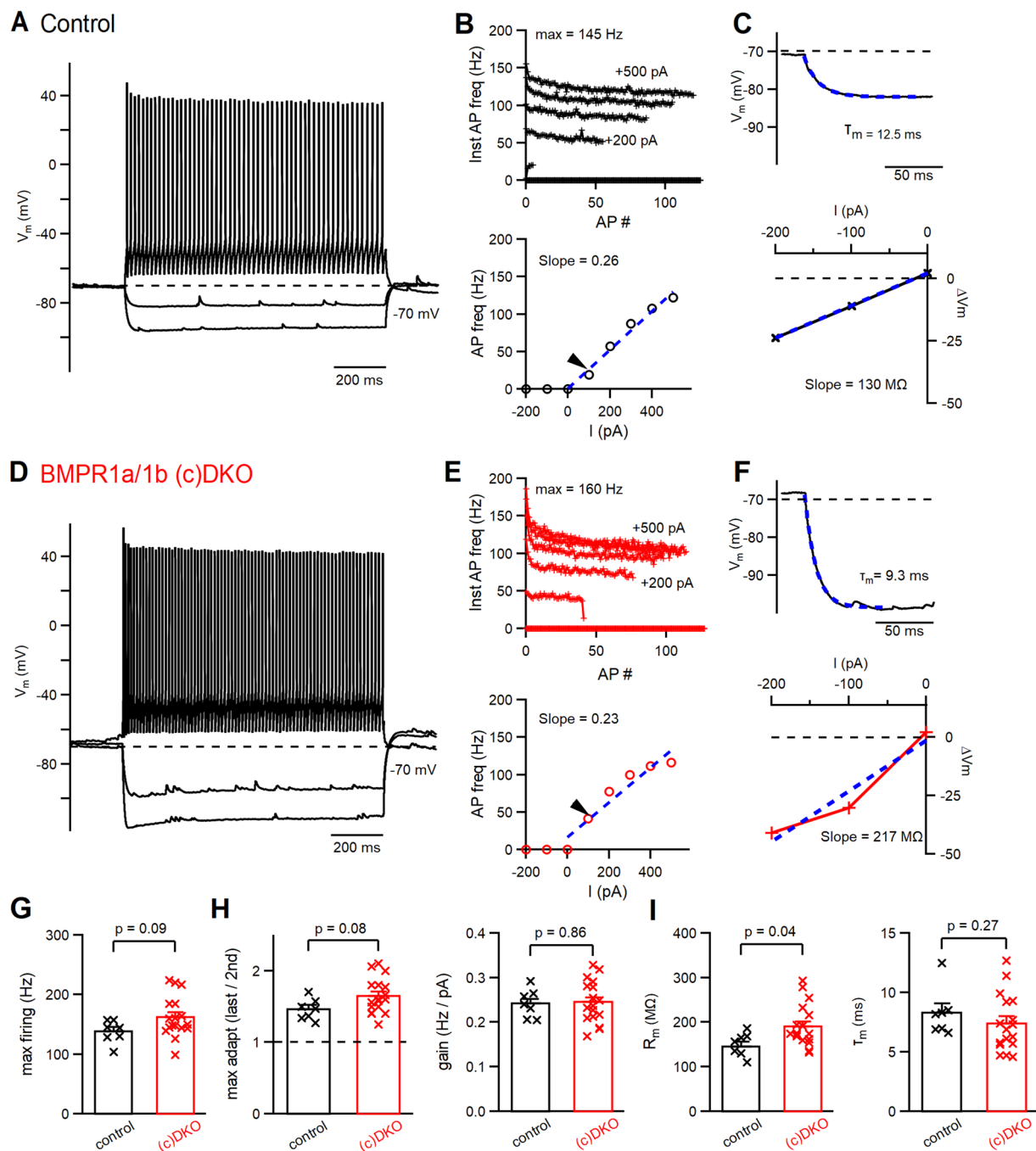


Figure 1. AP-firing properties and passive membrane properties of PV-INs are largely unchanged in BMPR1a/1b (c)DKO mice. **(A)** AP-firing of a PV-IN in a control mouse of age P22, in response to 1-s current steps to -200, -100 and +200 pA. **(B)** Instantaneous AP frequency (top) and plot of AP-frequency as a function of injected current (bottom). **(C)** Exponential fit (dashed blue line) to the membrane potential (V_m) relaxation caused by a -100 pA current injection, to determine the membrane time constant (τ_m ; top), and plot of the steady-state V_m value as a function of the injected current to determine membrane resistance (slope = 130 M Ω in this example). The data in **(A–C)** are from the same recording. **(D–F)** Same as **(A–C)**, but for a recording of a PV-IN in a BMPR1a/1b (c)DKO mouse of age P19. **(G)** Individual - and average data of the maximal AP firing frequency in control mice (left, black data points) and in BMPR1a/1b (c)DKO mice (right, red data points). **(H)** Individual - and average data for maximal adaptation (left), and for the firing rate gain (right). The latter was calculated as the slope in the plots of AP-firing versus injected current (**B,E**, bottom). **(I)** Individual - and average data for membrane resistance (left) and membrane time constant (right). For the number of recordings (n) and number of mice (N), and the statistical tests used, see Results.

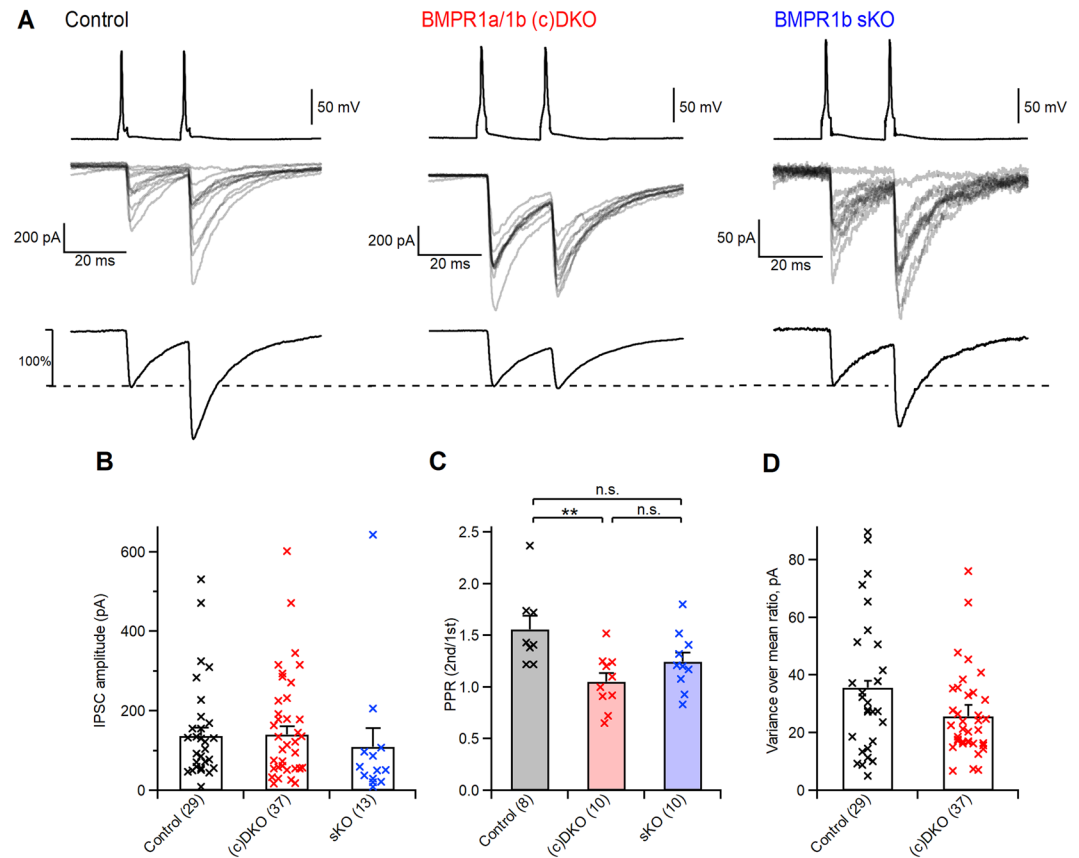


Figure 2. Knock-out of BMP-type1 receptors in PV-INs leads to an increased release probability, but does not affect baseline synaptic transmission at PV-IN output synapses. **(A)** APs evoked by brief current injections in PV-INs (V_m traces on top), and the resulting IPSCs in a postsynaptic principal neuron of layer 4 (middle). The bottom panels show peak-normalized IPSCs averaged from a larger number of stimulations ($n = 40-60$). From left to right, example paired recording from a control mouse at P23, from a BMPR1a/1b (c)DKO mouse at P21, and from a BMPR1b sKO at P22. **(B)** Individual - and average values of unitary IPSC amplitudes recorded in paired recordings in control mice (left); in BMPR1a/1b (c)DKO mice (middle) and in BMPR1b sKO mice (right). A Kruskal-Wallis test did not find a significant difference between the groups (see Results). **(C)** Individual - and average data for paired-pulse ratio (PPR) in a subset of recordings in which paired stimulation was applied, for the same genotypes as in **(B)**. **(D)** Individual- and average values of the IPSC variance - mean ratio of the IPSC peak amplitudes, in control mice (left) and in BMPR1a/1b (c)DKO mice (right). In panels **(B-D)**, the number of recordings (“ n ”) is indicated on the x-axis; for the number of animals (“ N ”) see Results. For statistical tests and p-values, see Results. ** $p < 0.01$; n.s., not significant.

the number of oligodendrocytes and Calbindin-positive interneurons³², and it was shown that exogenous BMP4 can act on PV-INs or their precursors to contribute to the morphological differentiation of PV-INs³³. However, it is unknown whether BMP signaling in PV-INs is necessary for the development of the functional properties of this class of interneurons. Here, we use genetic tools, patch-clamp recordings and single-cell gene expression analyses to address this question.

Results

Fast firing properties of PV-INs are largely independent of BMP-signaling. Mature PV-INs can sustain high-frequency AP firing, and show fast release kinetics and spike-timing dependent plasticity at their output synapses (see Introduction). To investigate whether the developmental acquisition of these functional properties depends on BMP-signaling in PV-INs, we genetically deleted two critical BMP-type 1 receptor subunits, BMPR1a and BMPR1b. We interbred a conventional BMPR1b KO mouse³⁴ with a conditional BMPR1a KO mouse (BMPR1a^{lox/lox}, ref. 35, targeted to PV-INs by the use of PV^{Cre} mice; ref. 36). To facilitate analysis, PV-INs were genetically labelled with a tdT reporter line (Ai9; see Materials and Methods). In the auditory cortex, onset of Cre-mediated recombination in PV^{Cre} mice occurs at ~P13. Therefore, we focused our analysis to an age of P19–P24. This age corresponds to a developmental period shortly after the critical period for the remodeling of sound frequency representation in primary auditory cortex at P11–P14^{37,38}. We assume that in (c)DKO mice, the removal of BMPR1a in the Cre-expressing PV-INs will, in the background of BMPR1b^{-/-} mice, lead to an arrest of BMP-signaling.

We recorded tdTomato-positive PV-INs in slices of primary auditory cortex of BMPR1a/1b (c)DKO mice, and in control littermate mice. Control mice had at least one functional allele of BMPR1a and -1b (see Materials and Methods). At the age investigated here, PV-INs in control mice exhibited high-frequency AP firing upon positive current injection, with maximal firing rates of 138 ± 7 Hz (Fig. 1A,B,G; $n = 7$ PV-INs). In PV-INs from BMPR1a/1b (c)DKO mice, the maximal firing frequency was higher (162 ± 8 Hz; Fig. 1D,E,G), but this trend did not reach statistical significance ($p = 0.09$; Fig. 1G; $n = 7$ and $n = 17$ recordings from $N = 7$ control - and $N = 13$ (c)DKO mice). Furthermore, curves of instantaneous AP-frequency versus AP number, and of time-averaged AP frequency versus injected current amplitude appeared similar between control- and (c)DKO mice (Fig. 1B,E). Accordingly, neither the maximal adaptation, nor the firing rate gain (i.e. slope of AP frequency versus injected current) were significantly different in BMPR1a/1b (c)DKO mice as compared to control mice (Fig. 1H; $p = 0.08$ and $p = 0.86$ respectively). Thus, fast AP firing of PV-INs, a property which must be acquired developmentally before the age recorded here, was not affected in BMPR1a/1b (c)DKO mice.

We furthermore analyzed the membrane resistance and membrane time constant using negative current injections. The membrane resistance was larger in BMPR1a/1b (c)DKO mice as compared to control (Fig. 1C,F), but this effect was moderate (an increase of $\sim 25\%$), and on the edge of statistical significance ($p = 0.04$; Fig. 1I, left). The membrane time constant was not different between the two genotypes (average values of ~ 8 ms in both genotypes; Fig. 1I, right; $p = 0.27$, Mann-Whitney's test). Taken together, neither the developmental acquisition of the high AP firing frequency in PV-INs, nor of their fast, subthreshold membrane potential signaling seemed to depend strongly on BMP-receptor signaling in these cells. Nevertheless, we cannot exclude that differences appear in BMPR1a/1b (c)DKO mice with further development.

Changes in release probability at the output synapses of PV-INs. We next investigated whether the properties of synaptic transmission at inhibitory synapses formed by PV-INs onto L4 principal neurons in auditory cortex are altered in the (c)DKO mice. We performed paired whole-cell recordings; PV-INs were identified by their tdTomato fluorescence, and postsynaptic principal neurons by their characteristic morphology and by their AP firing properties¹¹. We found that unitary IPSCs in control mice covered a large range of amplitudes across paired recordings (~ 10 – 500 pA), with an average amplitude of 149 ± 23 pA ($n = 29$; $N = 18$; Fig. 2A,B, left), in good agreement with previous work¹¹. In BMPR1a and -1b (c)DKO mice, the unitary IPSC amplitude also covered a large range, with an average value of 157 ± 21 pA ($n = 37$; $N = 24$), that was indistinguishable from the IPSC amplitude in control mice. We furthermore investigated BMPR1b single KO mice (sKO). This was necessary to control for non-specific effects that might result from the constitutive deletion of BMPR1b from cells other than PV-INs in the cortical network. The unitary IPSC amplitude in BMPR1b sKO mice was 109 ± 46 pA ($n = 13$ and $N = 6$), and a Kruskal-Wallis test reported no significant effect of genotype across the three groups ($p = 0.99$, Fig. 2B). Thus, the baseline strength of synaptic transmission at the PV-IN to principal neuron synapse was unchanged upon removal of BMPR1a and -1b from PV-INs.

In a subset of recordings, we evoked a second presynaptic AP at an interval of 20 ms to study the paired-pulse ratio of synaptic transmission, as an indicator of presynaptic release probability (PPR; defined as $IPSC_2/IPSC_1$). We found that PPR was decreased in BMPR1a/1b (c)DKO mice (Fig. 2A, bottom; Fig. 2C). ANOVA showed that PPR was significantly different across the three genotype groups ($p = 0.0073$). Further post-hoc statistical testing showed that (c)DKO mice and control mice had significantly different PPR ($p = 0.005$; Tukey's post-hoc test). This finding suggests that the release probability at PV-IN output synapses of (c)DKO mice is increased. In BMPR1b sKO mice, the PPR was in-between the values for control mice and (c)DKO mice, but not significantly different from neither of them ($p = 0.1$ and 0.35 respectively; Tukey's post-hoc test). These data indicate that the conditional removal of BMPR1a from PV-INs (in the background of the BMPR1b sKO mice) caused the observed changes in PPR.

An increased release probability is expected to cause an increased unitary IPSC amplitude, if other quantal parameters of transmission had been unchanged. Nevertheless, in the overall dataset, the unitary IPSC amplitude was indistinguishable between control-, and BMPR1a/1b (c)DKO mice (see above; Fig. 2B). A masking of the effects of a changed release probability could be caused by small opposing effects of either the quantal size q , and/or of the readily-releasable vesicle pool available at the PV-IN to L4 principal neuron connection. To test for such changes, we performed a variance - mean analysis, using baseline IPSC data obtained at stimulation frequency of 0.1 Hz (see below, Fig. 3A–C for examples). We found that the variance - mean value was 36 ± 4 pA ($n = 29$ and $N = 18$) and 26 ± 2 pA ($n = 37$ and $N = 24$) in control- and BMPR1a/1b (c)DKO mice, but this trend did not reach statistical significance ($p = 0.1$; Mann-Whitney test). In principle, a smaller variance - mean ratio would indicate a lower quantal amplitude q . Nevertheless, a small decrease in IPSC variance would also be expected for a reduced readily-releasable pool^{39,40}.

Deficient spike-timing dependent iLTP in the absence of BMP-signaling in PV-INs. We next investigated spike-timing dependent long-term plasticity at the inhibitory synapses formed by PV-INs onto L4 principal neurons¹¹. After establishing a baseline unitary IPSC amplitude for a given paired recording (Fig. 3A, left), we applied repeated AP stimuli in the postsynaptic - then presynaptic order at an interval of 5 ms (50 times, 0.2 Hz; "post-pre induction"; Fig. 3A, middle). This induced a long-lasting potentiation of the unitary IPSC amplitude by $40 \pm 8\%$ ($n = 9$, $N = 6$; Fig. 3D, left), similar to previous results¹¹. In the BMPR1a/1b (c)DKO mice, the same protocol failed to induce LTP of inhibition in most recordings (Fig. 3B), and occasionally caused long-term depression (LTD) of inhibition. Because the amount of plasticity observed in (c)DKO mice was close to zero in many recordings, we next performed a statistical analysis to determine if the change in IPSC amplitude after the induction protocol was significant. This revealed that in recordings from BMPR1a/1b (c)DKO mice, the change in IPSC amplitudes was in most cases not significant ($p > 0.05$, unpaired t-test; see Fig. 3D, dataset in the middle, open circles; $n = 7$ out of $n = 8$ recordings). Conversely, in the recordings from control mice, significant iLTP was

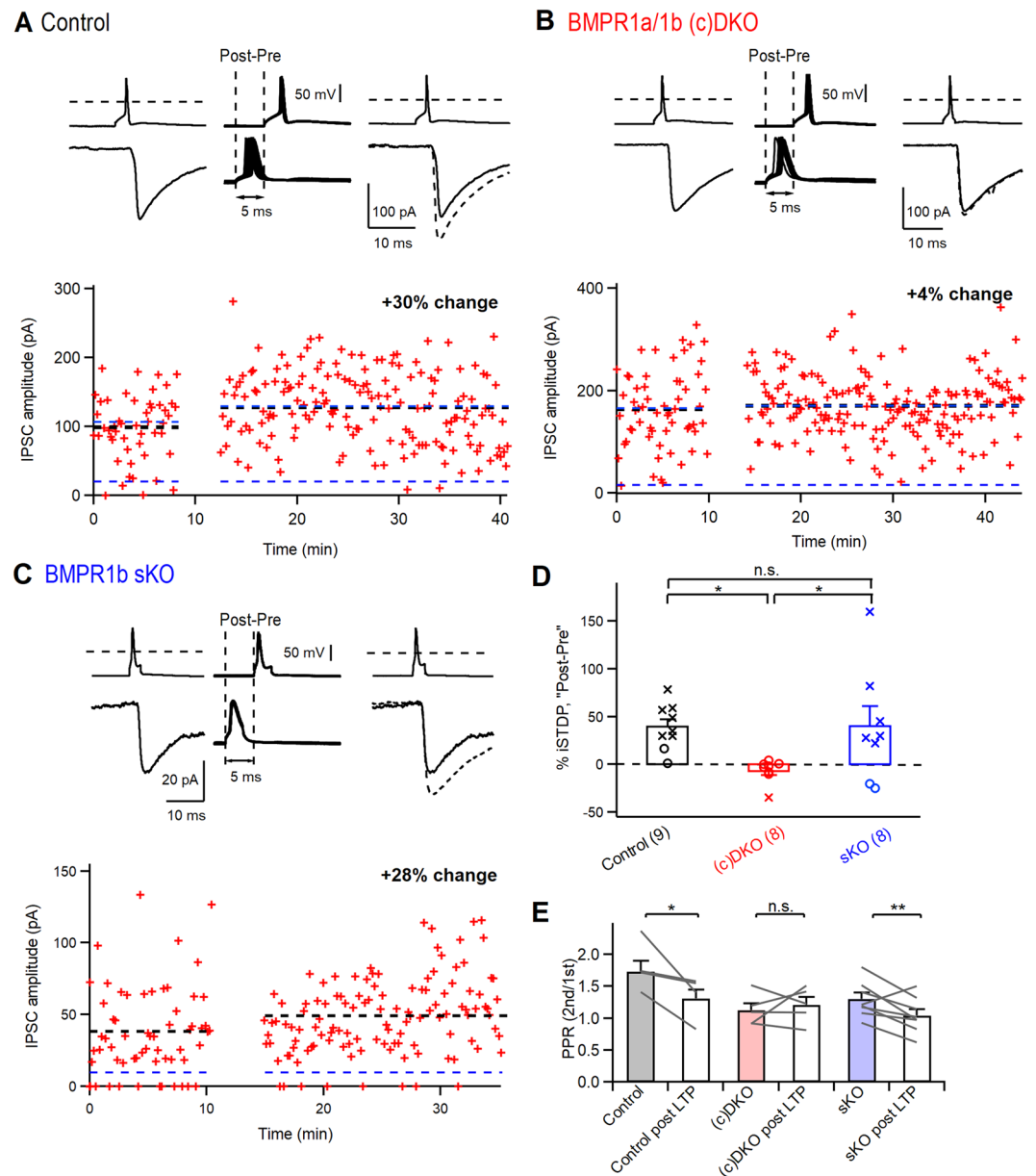


Figure 3. Knock-out of BMP-type 1 receptors in PV-INs impairs spike-timing dependent LTP at PV-IN output synapses. (A–C) Example of spike-timing dependent plasticity experiments with “post - pre” AP stimulation in paired recordings from a control mouse at P21 (A), from a BMPR1a/1b (c)DKO mouse at P20 (B), and from a BMPR1b sKO mouse at P21 (C). The traces on the top of each panel show presynaptic APs (in mV; top), and postsynaptic IPSCs during baseline (left, in [pA]), pre- and postsynaptic APs during the induction of spike-timing dependent plasticity (middle, in mV), and again IPSCs and presynaptic APs after the induction period (right, in [pA], same scale as left). Continuous IPSC traces represent average IPSCs during baseline; dashed IPSC traces represent the average IPSCs during the post-induction period. The plots on the bottom are IPSC stability plots. Thick dashed lines represent the average IPSC amplitude for baseline - and post-induction times. The amount of spike-timing dependent plasticity for each example is indicated. The lower thin dashed lines represent the threshold amplitude below which IPSCs were regarded as failures (see ref. ¹¹). (D) Individual - and average values of spike-timing dependent plasticity measured in control mice (left, black data points), in BMPR1a/1b (c)DKO mice (middle, red data points), and in BMPR1b sKO mice (right, blue data points). Significantly - and non-significantly changed IPSC amplitudes are indicated by cross - and open symbols, respectively (t-test; $p < 0.05$ and $p > 0.05$ respectively). For the statistics of the group comparisons, and for n and N numbers, see Results. (E) Individual - and average values of PPR for a subset of recordings in which paired presynaptic stimuli were given. For each genotype, PPR under baseline conditions (left bar with color), and following the induction of spike-timing dependent plasticity (right open bar) is given. Left two bars, data from $n = 4$ recordings in control mice; middle two bars, data from $n = 5$ recordings in BMPR1a/1b (c)DKO mice; right two bars, data from $n = 8$ BMPR1b sKO mice. ** $p < 0.01$; * $p < 0.05$; n.s., not significant.

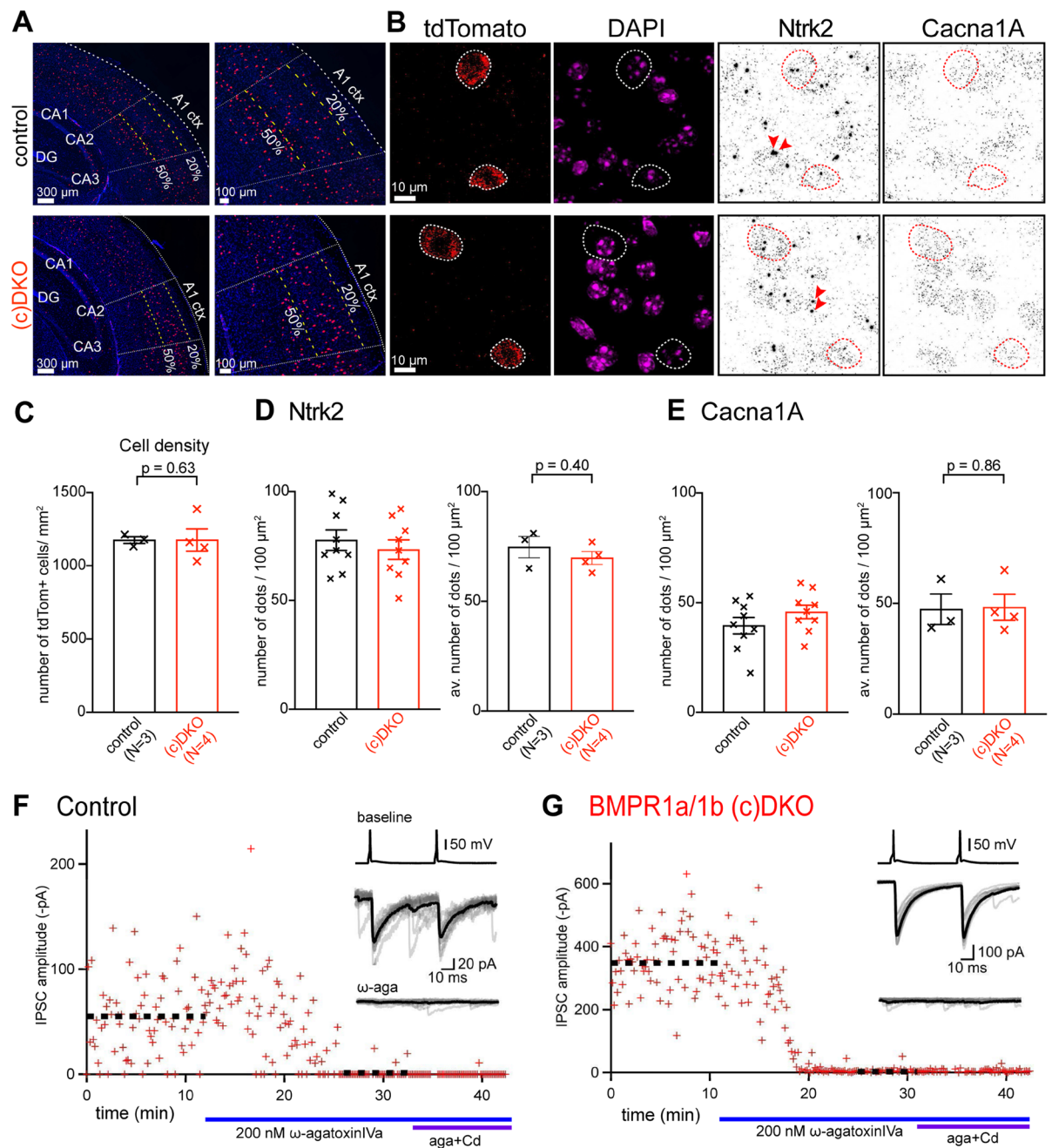


Figure 4. Expression levels of TrkB and P/Q-type Ca^{2+} channels are unchanged in PV-INs of BMPR1a/1b (c) DKO mice. **(A)** FISH images of coronal brain sections at two magnifications (left, and right), for a control mouse at P25 (bregma, ~ -2.1 mm), and for a BMPR1a/1b (c)DKO mouse at P25 (bregma, ~ -2.4 mm). The red and the blue channels show the FISH probe for tdTomato (indicating PV-INs) and DAPI, respectively. “A1 ctx”, auditory cortex. **(B)** FISH images at higher magnification for a control mouse at P25 (top) and for a BMPR1a/1b (c)DKO mouse at P25 (bottom), showing, from left to right, the tdTomato probe channel with two PV-positive neurons each, the DAPI channel, the Ntrk2 channel, and the Cacna1A probe channel. Red arrowheads show nascent transcripts of Ntrk2 in the nucleus which were excluded from the quantifications. **(C)** The density of PV-INs within 20–50% depth of auditory cortex was unchanged between $N = 3$ control mice (left, black data points), and $N = 4$ BMPR1a/1b (c)DKO mice (right, red data points). **(D)** Left, individual - and average data of the normalized number of Ntrk2 transcript dots for $n = 9$ PV-INs each from a control mouse (black data points), and from a BMPR1a/1b (c) DKO mouse (red data points). Right, averaged data from $N = 3$ control mice (left) and from $N = 4$ BMPR1a/1b (c)DKO mice (right). **(E)** Similar data as in **(D)**, here for Cacna1A transcript levels, the gene which codes for the α -subunit of the P/Q-type Ca^{2+} channel. **(F,G)** Example paired recordings in which the P/Q-type Ca^{2+} channel blocker ω -agatoxinIVa (200 nM) was applied, followed by the application of the same toxin plus $100 \mu\text{M}$ CdCl_2 . Note that unitary IPSCs are almost completely blocked by ω -agatoxin-IVa in both genotypes. The inset shows traces of presynaptic APs (top, only for control conditions), and of postsynaptic IPSCs before - (middle) and after application of ω -agatoxinIVa (bottom). For statistical analysis and number of recordings, see Results.

observed in $n = 8$ out of $n = 9$ recordings ($p < 0.05$, unpaired t-test; Fig. 3D, data set on the left, cross symbols). The group average revealed a decrease in IPSC amplitude to $-6 \pm 4\%$ in (c)DKO mice ($n = 8$, $N = 6$; Fig. 3D, middle). In the BMPR1b sKO mice, LTP was indistinguishable from that of control mice (Fig. 3C,D, right; $n = 8$, $N = 5$). ANOVA reported a significant effect of genotype on iLTP (Fig. 3D; $p = 0.027$). Tukey's post-hoc test found that the magnitude of iLTP was significantly smaller in BMPR1a/1b (c)DKO mice as compared to control mice ($p = 0.044$), and as compared to the BMPR1b sKO mice ($p = 0.046$; Fig. 3D). These findings suggest that BMP-receptor signaling in PV-INs at $\sim P15 - P20$ is a pre-requisite for the development of cellular mechanisms that enable spike-timing dependent LTP at PV - IN output synapses.

In a subset of the recordings, we again applied paired stimuli to measure possible changes in PPR after the induction of LTP. In the control mice, the PPR was significantly reduced after the induction of LTP ($p = 0.046$, $n = 4$; Fig. 3E, left), consistent with a presynaptic locus of expression for LTP of inhibition¹¹. In (c)DKO mice, the PPR was not significantly changed after the induction protocol ($p = 0.39$, $n = 5$; Fig. 3E, middle), consistent with an absence of LTP in this genotype (Fig. 3D). Furthermore, the PPR before induction was smaller than in the control mice (see also Fig. 2C). Finally, in BMPR1b sKO mice, the PPR was decreased by LTP induction ($p = 0.008$, $n = 8$ Fig. 3E, right). These findings are consistent with the notion of an increased release probability in BMPR1a/1b (c)DKO mice (Fig. 2C), and that this increased release probability could occlude the expression of LTP at the output synapses of PV-INs.

Expression of TrkB is unchanged in PV-INs of BMPR1a/1b (c)DKO mice. Activation of BMP-receptors modifies gene expression in target cells by SMAD-dependent signaling cascades⁴¹. In BMPR1a/1b (c)DKO mice, we observed alterations in presynaptic release probability and of LTP at PV-IN output synapses (Figs. 2 and 3). Transmitter release at PV-IN output synapses is mediated by P/Q-type Ca^{2+} channels^{42,43}, and spike-timing dependent LTP of inhibition involves retrograde BDNF signaling from principal neurons onto nerve terminals of PV-INs¹¹. Thus, we probed whether the mRNA levels coding for the P/Q - type Ca^{2+} channel subunit α -1A (Cacna1A) and for the BDNF receptor TrkB (Ntrk2) might be altered in BMPR1a/1b (c)DKO mice. We used fluorescent *in-situ* hybridization (FISH) on sections from control - and (c)DKO mice; PV-INs were detected with a tdTomato FISH probe based on the Cre-dependent expression of this reporter gene in PV-INs. We found that the density of PV-INs in the auditory cortex was unchanged in BMPR1a/1b (c)DKO mice as compared to control mice (Fig. 4A,C). To investigate the mRNA expression levels of Cacna1a and Ntrk2, we counted the puncta within the somata of tdTomato - positive neurons (Fig. 4B). In $n = 9$ cells analyzed from one control - and one (c)DKO mouse each, we did not observe a difference in the number of puncta normalized by cell surface (Fig. 4D, left). Repeated measurements in $n = 32$ cells from $N = 3$ control mice, and in $n = 35$ cells from $N = 4$ BMPR1a/1b (c)DKO mice, did not indicate a significant change in the expression of Ntrk2 in PV-INs (Fig. 4D right, $p = 0.4$; Mann-Whitney test). Similarly, the mRNA expression of Cacna1a was unchanged between control mice, and BMPR1a/1b (c)DKO mice (Fig. 4E; $p = 0.86$; Mann-Whitney test).

To further test for the functional expression of presynaptic P/Q-type Ca^{2+} channels at the nerve terminals of PV-INs, we measured unitary IPSCs in paired recordings, and applied the specific P/Q-type Ca^{2+} channel toxin ω -agatoxin-iva⁴⁴. We found that the block of synaptic transmission by ω -agatoxin was unchanged between control - and BMPR1a/1b (c)DKO mice ($97 \pm 1.5\%$, $n = 2$; and $97 \pm 1.0\%$, $n = 6$; $p = 0.99$; Fig. 4F,G). Thus, consistent with unaltered Cacna1A transcript levels, P/Q-type Ca^{2+} channels continue to be the predominant Ca^{2+} channels at the output synapses of PV-INs of BMPR1a/1b (c)DKO mice.

Discussion

Layer 4 of sensory cortices receives information from thalamus via excitatory synapses on principal neurons, and this thalamocortical drive activates a powerful feedforward inhibition mediated by PV-INs^{7,8}. In the input layers of auditory cortex, the timing of AP firing is relevant⁴⁵⁻⁴⁷, and marked spike-timing dependent plasticity occurs both at excitatory synapses⁴⁸, and at inhibitory synapses formed by PV-INs onto principal neurons in layer 4 of the auditory cortex¹¹. In the auditory cortex of rodents, exposure to a predominant sound frequency during a critical period at P11–P14 leads to enhanced representation of that sound frequency^{11,37,38}. We previously found that at an age immediately following the critical period (P15–P22), induction protocols with opposite AP sequences (pre - post *versus* post - pre) cause opposing directions of long-term plasticity at the output synapses of PV-INs¹¹. Upon further development, at an age of 4–5 weeks, however, both spike-timing sequences cause long-term *potentiation* at the PV-IN output synapses¹¹. Thus, the direction of plasticity at the output synapses of PV-INs is developmentally regulated, and a symmetric learning rule of potentiation of inhibition is attained in more mature animals. A symmetric learning rule with potentiation of inhibition is, in turn, expected to stabilize neuronal networks⁴⁹. Nevertheless, the molecular mechanisms that drive the developmental changes of long-term plasticity at inhibitory synapses have been unknown.

Previous work showed that BMP signaling occurs in developing PV-INs and contributes to the morphological differentiation of PV-INs³³, but the effects of interrupting BMP signaling on the functional properties of PV-INs had not been studied. We used conditional genetic inactivation of BMPR1a in PV-INs, in the background of BMPR1b sKO mice, and studied these mice at P19–P24, about 7–10 days after the onset of Cre-expression in PV-INs at $\sim P13$. In BMPR1a/1b (c)DKO mice, there were no consistent effects on the passive membrane properties of PV-INs, nor on the high rate of AP-firing that these neurons can generate (Fig. 1). On the other hand, spike-timing dependent LTP of inhibition upon post - pre induction protocols was absent, and there was a concomitant reduction of PPR indicating an increased release probability at the output synapses of PV-INs (Figs 2, 3). In BMPR1b single KO mice, no deficits of LTP of inhibition were observed (Fig. 3D). These data show that developmental BMP-signaling in PV-INs determines presynaptic properties of the output synapses of PV-INs, including release probability, and spike-timing dependent long-term potentiation.

Given a role of BMP-signaling in determining the properties of the output synapses of PV-INs, it is tempting to speculate in which neuronal compartments of PV-INs BMP-receptors are localized, and which is the source of BMP that activates these receptors. At the drosophila neuromuscular junction, evidence for a retrograde BMP signaling direction from postsynaptic - to presynaptic compartments was obtained by genetic approaches^{31,50}. However, because of a lack of suitable antibodies for immunohistochemistry of BMP-receptors, we have not been able to study the localization of BMP-type 1 receptors in PV-INs. Single-cell genome-wide expression data suggests that BMPR1b is strongly expressed in astrocytes but only weakly expressed in various neuron types, whereas BMPR1a is more strongly expressed in neurons, including PV-INs (see <https://www.brainrnaseq.org/> established by ref. ⁵¹, and <http://greenberg.hms.harvard.edu/project/gene-database/> established by ref. ⁵²). This might suggest that amongst the two type-1 BMP-receptors investigated here, BMPR1a is mainly responsible for initiating BMP-signaling in PV-INs early postnatally; however, further experiments with the single conditional KO are necessary to reinforce this conclusion.

We have previously found that LTP of inhibition involves the activation of TrkB receptors, most likely localized on the presynaptic nerve terminals of PV-INs¹¹. Previous work has also shown that BDNF signaling can influence critical period plasticity by acting on inhibitory neurons in the visual cortex⁵³. Furthermore, earlier *in-vitro* experiments have reported that BMPs and neurotrophins, such as BDNF and NT3, can act synergistically in neurons⁵⁴, and that BMP2 can increase the expression of the NT3 receptor TrkC in peripheral neurons^{22,55,56}. For these reasons, we started to investigate whether Ntrk2, the gene coding for TrkB, shows a misregulated expression on the mRNA level in PV-INs of BMPR1a/1b (c)DKO mice. However, we did not find significant changes in transcript levels of Ntrk2 in PV-INs of BMPR1a/1b (c)DKO mice (Fig. 4). Nevertheless, it remains possible that BMP-signaling in PV-INs regulates the expression level of TrkB on the protein level, and/or that a scaffolding protein necessary for the correct subcellular localization and function of the BDNF receptor TrkB is regulated by BMP-signaling in PV-INs.

We also analyzed the expression of *Cacna1a*, the gene which codes for the α -subunit of voltage-gated P/Q type Ca^{2+} channels. P/Q-type Ca^{2+} channels are expressed in PV-INs both on the soma-dendritic compartment and at the nerve terminal^{42,43,57,58}. We found that the mRNA levels of *Cacna1A* were not changed significantly in PV-INs, and correspondingly, synaptic transmission at the output synapses of PV-INs continued to be highly sensitive to the P/Q-type Ca^{2+} channel blocker ω -agatoxin-IVA (Fig. 4). Thus, the target genes downstream of BMP- and SMAD-signaling in PV-INs need to be systematically investigated in future studies, possibly using genome-wide screening approaches. Identifying target genes whose expression is regulated by BMP-signaling in PV-INs might allow further insights into the signaling pathways that enable a presynaptic, BDNF-dependent form of LTP at the output synapses of these interneurons¹¹.

PV-INs are characterized by the high AP firing frequency they can sustain⁵, a property which is acquired during postnatal development^{15,16}. We did not find clear effects on the high AP firing frequency that these neurons can support, nor on the membrane time constant of PV-INs in BMPR1a/1b (c)DKO mice (Fig. 1). The input resistance of PV-INs was moderately increased in BMPR1a/b (c)DKO mice (Fig. 11), which might suggest a slower developmental maturation towards a low membrane resistance in adult animals¹⁵.

Taken together, we find that developmental BMP-signaling in PV-INs determines presynaptic properties of the output synapses of these interneurons, including release probability and spike-timing dependent LTP of inhibition. A symmetric “learning rule” of long-term *potentiation* of inhibition regardless of the exact sequence of pre- and postsynaptic APs is established at ~P28 (ref. ¹¹), and a symmetric learning rule is likely beneficial for the stability of neuronal networks⁴⁹. Thus, it is possible that developmental BMP-signaling in PV-INs, which supports LTP of inhibition, is a prerequisite for certain types of homeostatic plasticity in cortical networks^{9,59}. This hypothesis could be tested in future systems-level investigations of cortical function using BMP-receptor mutants.

Materials and Methods

Ethics statement. All experiments with laboratory mice followed the guidelines and regulations of the Swiss Federal law on the protection of animals (“Loi fédérale sur la protection des animaux”). The specific experimental procedures with laboratory mice were approved by the SCAV (Service of Consumption and Veterinary Affairs, Canton of Vaud, Switzerland; authorizations VD2063.3, VD2063.4).

Mouse pups were kept in the homecage with their mother; weaning was done at P25. One mouse at a time, at age P19 to P24, was carefully removed from the cage, and killed by decapitation either without prior anesthesia, or after a brief isoflurane anesthesia in later experiments (protocols approved by the SCAV).

Mouse lines. We wished to inactivate BMP-signaling in PV-INs, by genetically deleting two essential BMP-type 1 receptors, BMPR1a and -1b. For this purpose, we generated a conditional/conventional double KO (DKO) mouse model of BMP-receptor (BMPR) 1a and 1b, based on an interbreeding of four mouse lines. (1) A conditional knock-out (KO) mouse line of the *Alk3* gene which codes for BMPR1a (*BMPR1a^{lox/lox}*; ref. ³⁵). (2) A conventional KO mouse of the *Alk6* gene which codes for BMPR1b (*BMPR1b^{-/-}*; ref. ³⁴). (3) A *PV^{Cre}* mouse line to drive Cre-expression in PV-INs (*PV^{Cre/+}*; ref. ³⁶). (4) A reporter mouse line driving the expression of tdTomato in Cre-expressing cells (*Ai9*; ref. ⁶⁰; called here “tdT”), which was used to target recordings to PV-INs and to guide cellular gene expression analyses. In breeding pairs that gave rise to mice used here, both males and females were heterozygous for the BMPR1a locus (*BMPR1a^{+/lox}*) and for the BMPR1b locus (*BMPR1b^{+/-}*), and homozygous in the PV locus (*PV^{mut/mut}*) and for the tdT transgene (*tdT^{mut/mut}*). The offspring of these breedings therefore showed the following genotypes: (1) Homozygous (c)DKO mice with genotype of *BMPR1a^{lox/lox}*, *BMPR1b^{-/-}*; this genotype is expected to occur at a fraction of 1/16. (2) Homozygous wild-type mice with genotype of *1a^{+/+}* [for *BMPR1a^{+/+}*], *1b^{+/+}* [for *BMPR1b^{+/+}*]; expected at a rate of 1/16. (3) Heterozygous animals with at least one functional allele of each BMP-type 1 receptor (i.e. genotypes *1a^{+/+}*, *1b^{+/-}* at 1/8; *1a^{+/lox}*, *1b^{+/-}* at 1/4; *1a^{lox/+}*, *1b^{+/+}* at 1/8). Because homozygous wild-type mice were difficult to obtain in this breeding scheme, we used mice with

at least one functional allele of each BMP type 1 receptor as “wild-type” controls (all genotypes listed in group (3) above). (4) Single KO (sKO) mice for the BMPR1b (genotypes, 1a^{+/+}, 1b^{-/-} at 1/16; 1a^{+lox}, 1b^{-/-} at 1/8); these mice were used to control for compensatory networks effects that might result from the constitutive inactivation of the BMPR1b allele (see Results). (5) Single conditional KO mice of the BMPR1a allele (genotypes, 1a^{lox/lox}, 1b^{+/-} at 1/8; 1a^{lox/lox}, 1b^{+/+} at 1/16) - these mice were not used for experiments. We observed that the genotype fractions roughly conformed with the expected Mendelian ratios, although in some cases fewer (c)DKO mice than expected seemed to be present by ~P6. For this reason, in early breedings, at least one parent was homozygous for BMPR1a^{lox}. Although (c)DKO mice could only be obtained at low numbers, the above breeding scheme had the advantage that all three mouse genotype groups were obtained from the same breedings (“wild-type” control mice, (c)DKO mice, and BMPR1b sKO mice).

Slice preparation and patch-clamp electrophysiology. We made patch-clamp recordings of PV-INs identified by their tdTomato fluorescence, either alone or together with a recording of a connected principal neuron, using an EPC10/2 patch-clamp amplifier (HEKA elektronik, Germany, see <https://www.heka.com/>). Recordings were made in slices of auditory cortex of young mice (P19–P24), at a depth of 30–50% from the cortical surface, which we regard as layer 4 (ref. ¹¹). By targeting tdTomato-positive neurons using PV^{Cre} mice, we assume that we target fast-firing, PV-positive basket cells, which are an abundant interneuron population in layer 4 of mouse auditory cortex⁶¹. However, because chandelier cells also express PV (ref. ⁶²), and have similar AP firing properties as basket cells⁶³, it remains possible that a minority of the sampled cells represent chandelier cells. We note, however, that in primary auditory cortex and other sensory cortices of mice, only few of the more complex nerve endings of chandelier cells were detected⁶⁴, and that in many cortical areas, the density of chandelier cells is low in layer 4.

Parahorizontal thalamocortical auditory slices (300 μ m) of mouse brain were made with a vibratome (Leica VT 1200). Whole-cell patch-clamp recordings were performed at room temperature (21–23 °C), in set-ups with an upright microscope (either Olympus BX51WI, or ZEISS Axioskop 2), equipped with 60 \times , 0.9 numerical aperture objectives (Olympus). The tdTomato fluorescence of genetically labeled PV-INs (tdT reporter mice; see above) was excited with a Polychrome V (or Polychrome IV; TILL Photonics) monochromator at 550 nm (using a 570–613 nm emission filter). Images were detected with a CCD camera (either Retiga 2000RV or PCO Sensicam).

The patch-pipette (intracellular) solution for recording PV-INs contained (in mM): 135 K-gluconate, 10 KCl, 0.5 HEPES, 5 Na₂-Phosphocreatine, 4 Mg-ATP, 0.3 Na₂-GTP, 0.5 EGTA. The pH was set to 7.2 by adding KOH, the osmolarity was ~305 mOsm. The patch pipette solution for recording postsynaptic principal neurons was similar to the above solution, but contained 160 mM KCl and no K-gluconate. Because of the high intracellular [Cl⁻], IPSCs were recorded as inward currents at a holding potential of -70 mV. The extracellular solution was a standard bicarbonate-buffered solution containing 2 mM CaCl₂ and 1 mM MgCl₂. For the measurement of spike-timing-dependent plasticity of IPSCs, the series resistance (R_s) of the postsynaptic recording was minimized, and R_s was verified regularly throughout the recording. A change in the R_s by more than \pm 50%, and above a value of 20 M Ω led to the exclusion of a recording from the final dataset.

For measurements of the AP-firing behavior and passive membrane properties in recordings of PV-INs alone (Fig. 1), 1 s current steps between -200 and +500 pA (increments of +100 pA) were applied in current-clamp experiments in single recordings. During paired recordings, unitary IPSCs between the PV-IN and a L4 principal neuron were first measured under baseline conditions, by applying short (3 ms) current steps in the PV-INs under current clamp to evoke single APs repeated every 10 s; the resulting postsynaptic IPSC was measured with a second patch-clamp amplifier under voltage-clamp at a holding potential of -70 mV. Following this baseline period, a spike-timing dependent plasticity protocol was applied, in which a postsynaptic AP was followed by a presynaptic AP (post - pre induction; see ref. ¹¹). Specifically, post- and presynaptic current injections (1 nA for 3 ms duration in both recordings) were applied with a time offset of 5 ms, 50 times every 5 s.

Fluorescent *in situ* hybridization. Fluorescence *in situ* hybridization (FISH) was performed using the RNAscope Fluorescent Multiplex Kit (ACD) protocol. Briefly, brains were dissected from P25 male and female mice and snap frozen in liquid nitrogen. Coronal sections (18 μ m thick) were cut with a cryostat between Bregma -2 and -3.6 mm to include auditory cortex, adhered to Superfrost ultra plus slides (Thermo Scientific) and stored at -80 °C. Sections were fixed for 30 min in 4% PFA and treated with Protease IV. Hybridization was for 2 hours at 40 °C. The following probes (50 \times dilution), coupled to specific fluorophores, were used in the same hybridization reaction: *Ntrk2* (C1 # 423611; coupled to Atto 550), *Cacna1A* (C2 # 493141; Alexa 488) and *tdTomato* (C3, # 317041; Atto 647). DAPI was used to identify the nuclei. Images were acquired with an upright LSM700 confocal microscope (Zeiss) using a 40 \times Apochromat objective in z-stacks (19–22 images, 0.4 μ m intervals), using laser lines of 405 nm (for exciting DAPI), of 488 nm (for Alexa 488), of 555 nm (for Atto 550), and of 639 nm (for Atto 647). PV-INs were identified based on the presence of the tdTomato probe signal, and the expression of TrkB and *Cacna1a* was analyzed in PV-INs contained in a depth of 20–50% of auditory cortex. A region of interest (ROI) was drawn to define the area of the cell soma. Thresholding for detection of the signal throughout the stacks and the number of pixels was done with Fiji software (<https://fiji.sc/>), using the TrackMate plugin (<https://imagej.net/TrackMate>). The number of puncta for each probe set were then counted with the TrackMate plugin in the ROI. The number of puncta in the ROI, normalized to the area, were used as a proxy for expression strength of a given probe. The density of tdTomato positive cells spanning from 20% to 50% depth of auditory cortex was quantified from images acquired on a Widefield Axio Scan Z1 slide scanner. Images were assembled using Fiji and Adobe Illustrator CS6 (<https://www.adobe.com/uk/products/illustrator.html>).

Analysis and statistics. Analysis of electrophysiological data was made with Igor.Pro (versions 6.37 and 7.0.8.1; <https://www.wavemetrics.com>), using custom-written functions. The membrane time-constant (τ_m) was measured by fitting a single exponential function to the relaxation of the membrane potential (V_m) trace in response to a 1 s, -100 pA current step. The instantaneous AP frequency was measured from the inter-AP intervals for all pairs of subsequent APs in response to 1 s current injections. The maximal adaptation was calculated as the last interspike interval (ISI) in the train divided by the second ISI in the train.

Statistical tests for the analysis of electrophysiological data were performed in GraphPad Prism 5.01 (<https://www.graphpad.com/scientific-software/prism/>). For repeated experiments, the number of recorded cells or cell pairs is reported as “n”, and the number of investigated mice as “N”. For experiments in which the control group and the BMPR1a/1b (c)DKO group were compared, we first performed a Shapiro-Wilk normality test to determine whether the data was normally distributed. For datasets which passed the normality test we performed an unpaired Student’s test to determine the statistical significance of the difference between the two groups. If one of the groups failed the normality test, we performed a non-parametric Mann-Whitney test for unpaired comparisons instead, as indicated in the Results. For the comparison of paired-pulse ratios (PPR) before- and after LTP induction in a given recording, we used paired Student’s t-test.

For experiments in which three groups of mice were compared, we used one-way ANOVA if all datasets passed the Shapiro-Wilk normality test. If one or more of the datasets failed the normality test, a non-parametric Kruskal-Wallis test was used, as indicated in the Results. In both cases, if the p value of the ANOVA/ Kruskal-Wallis test was below 0.05, we performed post hoc tests, corrected for multiple comparisons. For parametric one-way ANOVA, we used the Tukey’s multiple comparisons test. In case of the non-parametric Kruskal-Wallis test, we used Dunn’s multiple comparisons test. In either case, alpha was set to 0.05.

Statistical tests for the quantifications of PV-IN cell density, TrkB and Cacna1A mRNA levels were performed in GraphPad Prism 8 (<https://www.graphpad.com/scientific-software/prism/>). The number of dots per cell were averaged to yield an average expression level in a given control- and (c) DKO mouse for both the TrkB- and Cacna1a probe. This analysis was repeated in a total of N = 3 control mice and N = 4 (c)DKO mice, and the statistical difference was tested with a non-parametric Mann-Whitney test for unpaired comparisons.

Data availability

The raw data leading to the conclusions of this paper can be found at Zenodo (10.5281/zenodo.3827171).

Received: 13 March 2020; Accepted: 27 May 2020;

Published online: 22 June 2020

References

- Rudy, B., Fishell, G., Lee, S. & Hjerling-Leffler, J. Three groups of interneurons account for nearly 100% of neocortical GABAergic neurons. *Developmental neurobiology* **71**, 45–61, <https://doi.org/10.1002/dneu.20853> (2011).
- Markram, H. *et al.* Reconstruction and Simulation of Neocortical Microcircuitry. *Cell* **163**, 456–492, <https://doi.org/10.1016/j.cell.2015.09.029> (2015).
- Zeisel, A. *et al.* Brain structure. Cell types in the mouse cortex and hippocampus revealed by single-cell RNA-seq. *Science* **347**, 1138–1142, <https://doi.org/10.1126/science.aaa1934> (2015).
- Tasic, B. *et al.* Shared and distinct transcriptomic cell types across neocortical areas. *Nature* **563**, 72–78, <https://doi.org/10.1038/s41586-018-0654-5> (2018).
- Hu, H., Gan, J. & Jonas, P. Interneurons. Fast-spiking, parvalbumin(+) GABAergic interneurons: from cellular design to microcircuit function. *Science* **345**, 1255263, <https://doi.org/10.1126/science.1255263> (2014).
- Kubota, Y. *et al.* Functional effects of distinct innervation styles of pyramidal cells by fast spiking cortical interneurons. *eLife* **4**, <https://doi.org/10.7554/eLife.07919> (2015).
- Gabernet, L., Jadhav, S. P., Feldman, D. E., Carandini, M. & Scanziani, M. Somatosensory integration controlled by dynamic thalamocortical feed-forward inhibition. *Neuron* **48**, 315–327, <https://doi.org/10.1016/j.neuron.2005.09.022> (2005).
- Cruikshank, S. J., Urabe, H., Nurmikko, A. V. & Connors, B. W. Pathway-specific feedforward circuits between thalamus and neocortex revealed by selective optical stimulation of axons. *Neuron* **65**, 230–245, <https://doi.org/10.1016/j.neuron.2009.12.025> (2010).
- Maffei, A., Nataraj, K., Nelson, S. B. & Turrigiano, G. G. Potentiation of cortical inhibition by visual deprivation. *Nature* **443**, 81–84, <https://doi.org/10.1038/nature05079> (2006).
- Lourenco, J. *et al.* Non-associative potentiation of perisomatic inhibition alters the temporal coding of neocortical layer 5 pyramidal neurons. *PLoS biology* **12**, e1001903, <https://doi.org/10.1371/journal.pbio.1001903> (2014).
- Vickers, E. D. *et al.* Parvalbumin-interneuron output synapses show spike-timing-dependent plasticity that contributes to auditory map remodeling. *Neuron* **99**(720–735), e726, <https://doi.org/10.1016/j.neuron.2018.07.018> (2018).
- Hensch, T. K. Critical period plasticity in local cortical circuits. *Nature reviews. Neuroscience* **6**, 877–888, <https://doi.org/10.1038/nrn1787> (2005).
- Kuhlman, S. J. *et al.* A disinhibitory microcircuit initiates critical-period plasticity in the visual cortex. *Nature* **501**, 543–546, <https://doi.org/10.1038/nature12485> (2013).
- Li, L., Gainey, M. A., Goldbeck, J. E. & Feldman, D. E. Rapid homeostasis by disinhibition during whisker map plasticity. *Proceedings of the National Academy of Sciences of the United States of America* **111**, 1616–1621, <https://doi.org/10.1073/pnas.1312455111> (2014).
- Doischer, D. *et al.* Postnatal differentiation of basket cells from slow to fast signaling devices. *J Neuroscience* **28**, 12956–12968 (2008).
- Okaty, B. W., Miller, M. N., Sugino, K., Hempel, C. M. & Nelson, S. B. Transcriptional and electrophysiological maturation of neocortical fast-spiking GABAergic interneurons. *The Journal of neuroscience: the official journal of the Society for Neuroscience* **29**, 7040–7052, <https://doi.org/10.1523/JNEUROSCI.0105-09.2009> (2009).
- Zhao, G. Q. Consequences of knocking out BMP signaling in the mouse. *Genesis* **35**, 43–56, <https://doi.org/10.1002/gene.10167> (2003).
- Dutko, J. A. & Mullins, M. C. Snapshot: BMP signaling in development. *Cell* **145**, 636, 636 e631–632, <https://doi.org/10.1016/j.cell.2011.05.001> (2011).
- Cardozo, M. J., Almuedo-Castillo, M. & Bovolenta, P. Patterning the Vertebrate Retina with Morphogenetic Signaling Pathways. *Neuroscientist*, 1073858419874016, <https://doi.org/10.1177/1073858419874016> (2019).
- Augsburger, A., Schuchardt, A., Hoskins, S., Dodd, J. & Butler, S. BMPs as mediators of roof plate repulsion of commissural neurons. *Neuron* **24**, 127–141 (1999).

21. Liu, A. & Niswander, L. A. Bone morphogenetic protein signalling and vertebrate nervous system development. *Nature reviews. Neuroscience* **6**, 945–954, <https://doi.org/10.1038/nrn1805> (2005).
22. Zhang, D., Mehler, M. F., Song, Q. & Kessler, J. A. Development of bone morphogenetic protein receptors in the nervous system and possible roles in regulating trkC expression. *The Journal of neuroscience: the official journal of the Society for Neuroscience* **18**, 3314–3326 (1998).
23. Sato, T., Mikawa, S. & Sato, K. BMP2 expression in the adult rat brain. *The Journal of comparative neurology* **518**, 4513–4530, <https://doi.org/10.1002/cne.22469> (2010).
24. Miyagi, M. *et al.* Bone morphogenetic protein receptor expressions in the adult rat brain. *Neuroscience* **176**, 93–109, <https://doi.org/10.1016/j.neuroscience.2010.12.027> (2011).
25. Kalinovsky, A. *et al.* Development of axon-target specificity of ponto-cerebellar afferents. *PLoS biology* **9**, <https://doi.org/10.1371/journal.pbio.1001013> (2011).
26. Higashi, T., Tanaka, S., Iida, T. & Okabe, S. Synapse elimination triggered by BMP4 exocytosis and presynaptic BMP receptor activation. *Cell reports* **22**, 919–929, <https://doi.org/10.1016/j.celrep.2017.12.101> (2018).
27. Xiao, L. *et al.* BMP signaling specifies the development of a large and fast CNS synapse. *Nature neuroscience* **16**, 856–864, <https://doi.org/10.1038/nn.3414> (2013).
28. Kronander, E., Clark, C. & Schneggenburger, R. Role of BMP Signaling for the Formation of Auditory Brainstem Nuclei and Large Auditory Relay Synapses. *Developmental neurobiology* **79**, 155–174, <https://doi.org/10.1002/dneu.22661> (2019).
29. Aberle, H. *et al.* wishful thinking encodes a BMP type II receptor that regulates synaptic growth in Drosophila. *Neuron* **33**, 545–558, doi:S0896627302005895 [pii] (2002).
30. Marques, G. *et al.* The Drosophila BMP type II receptor Wishful Thinking regulates neuromuscular synapse morphology and function. *Neuron* **33**, 529–543, doi:S0896627302005950 [pii] (2002).
31. McCabe, B. D. *et al.* The BMP homolog Gbb provides a retrograde signal that regulates synaptic growth at the Drosophila neuromuscular junction. *Neuron* **39**, 241–254, doi:S0896627303004264 [pii] (2003).
32. Samanta, J. *et al.* BMPRIa signaling determines numbers of oligodendrocytes and calbindin-expressing interneurons in the cortex. *The Journal of neuroscience: the official journal of the Society for Neuroscience* **27**, 7397–7407 (2007).
33. Mukhopadhyay, A., McGuire, T., Peng, C. Y. & Kessler, J. A. Differential effects of BMP signaling on parvalbumin and somatostatin interneuron differentiation. *Development* **136**, 2633–2642 (2009).
34. Yi, S. E., Daluiski, A., Pederson, R., Rosen, V. & Lyons, K. M. The type I BMP receptor BMPRI is required for chondrogenesis in the mouse limb. *Development* **127**, 621–630 (2000).
35. Mishina, Y., Hanks, M. C., Miura, S., Tallquist, M. D. & Behringer, R. R. Generation of Bmpr/Alk3 conditional knockout mice. *Genesis* **32**, 69–72 (2002).
36. Hippenmeyer, S. *et al.* A developmental switch in the response of DRG neurons to ETS transcription factor signaling. *PLoS biology* **3**, e159, <https://doi.org/10.1371/journal.pbio.0030159> (2005).
37. de Villers-Sidani, E., Chang, E. F., Bao, S. & Merzenich, M. M. Critical period window for spectral tuning defined in the primary auditory cortex (A1) in the rat. *J. Neuroscience* **27**, 180–189, <https://doi.org/10.1523/JNEUROSCI.3227-06.2007> (2007).
38. Barkat, T. R., Polley, D. B. & Hensch, T. K. A critical period for auditory thalamocortical connectivity. *Nature neuroscience* **14**, 1189–1194, <https://doi.org/10.1038/nn.2882> (2011).
39. Clements, J. D. & Silver, R. A. Unveiling synaptic plasticity: a new graphical and analytical approach. *TINS* **23**, 105–113 (2000).
40. Meyer, A. C., Neher, E. & Schneggenburger, R. Estimation of quantal size and number of functional active zones at the calyx of Held synapse by nonstationary EPSC variance analysis. *The Journal of neuroscience: the official journal of the Society for Neuroscience* **21**, 7889–7900 (2001).
41. Miyazono, K., Kamiya, Y. & Morikawa, M. Bone morphogenetic protein receptors and signal transduction. *Journal of biochemistry* **147**, 35–51, <https://doi.org/10.1093/jb/mvp148> (2010).
42. Hefft, S. & Jonas, P. Asynchronous GABA release generates long-lasting inhibition at a hippocampal interneuron-principal neuron synapse. *Nature neuroscience* **8**, 1319–1328, <https://doi.org/10.1038/nn1542> (2005).
43. Zaitsev, A. V., Povyshva, N. V., Lewis, D. A. & Krimer, L. S. P/Q-type, but not N-type, calcium channels mediate GABA release from fast-spiking interneurons to pyramidal cells in rat prefrontal cortex. *Journal of neurophysiology* **97**, 3567–3573, <https://doi.org/10.1152/jn.01293.2006> (2007).
44. Iwasaki, S., Momiyama, A., Uchitel, O. D. & Takahashi, T. Developmental changes in calcium channel types mediating central synaptic transmission. *J. Neurosci.* **20**, 59–65 (2000).
45. Wehr, M. & Zador, A. M. Balanced inhibition underlies tuning and sharpens spike timing in auditory cortex. *Nature* **426**, 442–446, <https://doi.org/10.1038/nature02116> (2003).
46. Zhou, Y. *et al.* Generation of spike latency tuning by thalamocortical circuits in auditory cortex. *J. Neuroscience* **32**, 9969–9980, <https://doi.org/10.1523/JNEUROSCI.1384-12.2012> (2012).
47. Moore, A. K. & Wehr, M. Parvalbumin-expressing inhibitory interneurons in auditory cortex are well-tuned for frequency. *J. Neuroscience* **33**, 13713–13723, <https://doi.org/10.1523/JNEUROSCI.0663-13.2013> (2013).
48. D'Amour, J. A. & Froemke, R. C. Inhibitory and excitatory spike-timing-dependent plasticity in the auditory cortex. *Neuron* **86**, 514–528, <https://doi.org/10.1016/j.neuron.2015.03.014> (2015).
49. Vogels, T. P., Sprekeler, H., Zenke, F., Clopath, C. & Gerstner, W. Inhibitory plasticity balances excitation and inhibition in sensory pathways and memory networks. *Science* **334**, 1569–1573, <https://doi.org/10.1126/science.1211095> (2011).
50. Ball, R. W. *et al.* Retrograde BMP signaling controls synaptic growth at the NMJ by regulating trio expression in motor neurons. *Neuron* **66**, 536–549, <https://doi.org/10.1016/j.neuron.2010.04.011> (2010).
51. Zhang, Y. *et al.* An RNA-sequencing transcriptome and splicing database of glia, neurons, and vascular cells of the cerebral cortex. *The Journal of neuroscience: the official journal of the Society for Neuroscience* **34**, 11929–11947, <https://doi.org/10.1523/JNEUROSCI.1860-14.2014> (2014).
52. Hrvatin, S. *et al.* Single-cell analysis of experience-dependent transcriptomic states in the mouse visual cortex. *Nature neuroscience* **21**, 120–129, <https://doi.org/10.1038/s41593-017-0029-5> (2018).
53. Huang, Z. J. *et al.* BDNF regulates the maturation of inhibition and the critical period of plasticity in mouse visual cortex. *Cell* **98**, 739–755 (1999).
54. Gratacos, E., Checa, N., Perez-Navarro, E. & Alberch, J. Brain-derived neurotrophic factor (BDNF) mediates bone morphogenetic protein-2 (BMP-2) effects on cultured striatal neurones. *Journal of neurochemistry* **79**, 747–755 (2001).
55. Kobayashi, M., Fujii, M., Kurihara, K. & Matsuoka, I. Bone morphogenetic protein-2 and retinoic acid induce neurotrophin-3 responsiveness in developing rat sympathetic neurons. *Brain research. Molecular brain research* **53**, 206–217 (1998).
56. Schnitzler, A. C. *et al.* BMP9 (bone morphogenetic protein 9) induces NGF as an autocrine/paracrine cholinergic trophic factor in developing basal forebrain neurons. *The Journal of Neuroscience* **30**, 8221–8228, <https://doi.org/10.1523/JNEUROSCI.5611-09.2010> (2010).
57. Rossignol, E., Kruglikov, I., van den Maagdenberg, A. M., Rudy, B. & Fishell, G. CaV 2.1 ablation in cortical interneurons selectively impairs fast-spiking basket cells and causes generalized seizures. *Ann Neurol* **74**, 209–222, <https://doi.org/10.1002/ana.23913> (2013).
58. Vecchia, D., Tottene, A., van den Maagdenberg, A. M. & Pietrobon, D. Mechanism underlying unaltered cortical inhibitory synaptic transmission in contrast with enhanced excitatory transmission in CaV2.1 knockin migraine mice. *Neurobiol Dis* **69**, 225–234, <https://doi.org/10.1016/j.nbd.2014.05.035> (2014).

59. Xue, M., Atallah, B. V. & Scanziani, M. Equalizing excitation-inhibition ratios across visual cortical neurons. *Nature* **511**, 596–600, <https://doi.org/10.1038/nature13321> (2014).
60. Madisen, L. *et al.* A robust and high-throughput Cre reporting and characterization system for the whole mouse brain. *Nat Neuroscience* **13**, 133–140, <https://doi.org/10.1038/nn.2467> (2010).
61. Levy, R. B. & Reyes, A. D. Spatial profile of excitatory and inhibitory synaptic connectivity in mouse primary auditory cortex. *J. Neuroscience* **32**, 5609–5619, <https://doi.org/10.1523/JNEUROSCI.5158-11.2012> (2012).
62. DeFelipe, J. & Gonzalez-Albo, M. C. Chandelier cell axons are immunoreactive for GAT-1 in the human neocortex. *Neuroreport* **9**, 467–470, <https://doi.org/10.1097/00001756-199802160-00020> (1998).
63. Taniguchi, H., Lu, J. & Huang, Z. J. The spatial and temporal origin of chandelier cells in mouse neocortex. *Science* **339**, 70–74, <https://doi.org/10.1126/science.1227622> (2013).
64. Inda, M. C., DeFelipe, J. & Munoz, A. Morphology and distribution of chandelier cell axon terminals in the mouse cerebral cortex and claustramygdaloid complex. *Cerebral cortex* **19**, 41–54, <https://doi.org/10.1093/cercor/bhn057> (2009).

Acknowledgements

We thank Heather Murray and Jessica Dupasquier (EPFL, Lausanne) for expert technical assistance, and for help with mouse breeding and genotyping, Caroline Bornmann (Biozentrum, University of Basel) for mouse brain histology and help with FISH experiments, and Laurent Guerard (Imaging Core Facility, IMCF, Biozentrum, Basel) for the analysis script used for FISH image analysis. Imaging was performed at the IMCF of Biozentrum, University of Basel. This work was supported by an SNSF Sinergia grant (CRSII3_154455 / 1) to both P.S. and R.S.

Author contributions

E.V., C.C. and R.S. designed the research. E.V., D.O. and C.C. performed and analyzed electrophysiological experiments. Z.O. performed FISH experiments; Z.O. and P.S. analyzed FISH experiments. E.V., P.S. and R.S. wrote the paper. E.V. and D.O. prepared Figures 1–3; Z.O. and D.O. prepared Figure 4. All authors reviewed the manuscript.

Competing interests

The authors declare no competing interests.

Additional information

Correspondence and requests for materials should be addressed to R.S.

Reprints and permissions information is available at www.nature.com/reprints.

Publisher's note Springer Nature remains neutral with regard to jurisdictional claims in published maps and institutional affiliations.



Open Access This article is licensed under a Creative Commons Attribution 4.0 International License, which permits use, sharing, adaptation, distribution and reproduction in any medium or format, as long as you give appropriate credit to the original author(s) and the source, provide a link to the Creative Commons license, and indicate if changes were made. The images or other third party material in this article are included in the article's Creative Commons license, unless indicated otherwise in a credit line to the material. If material is not included in the article's Creative Commons license and your intended use is not permitted by statutory regulation or exceeds the permitted use, you will need to obtain permission directly from the copyright holder. To view a copy of this license, visit <http://creativecommons.org/licenses/by/4.0/>.

© The Author(s) 2020